ACS OMEGA

http://pubs.acs.org/journal/acsodf

Article

Digital Protein Detection in Bulk Solutions

Sungjun Beck, Donghae Shin, Sun Jin Kim, Per Niklas Hedde,* and Weian Zhao*

Cite This: *ACS Omega* 2022, 7, 37714–37723

Read Online

ACCESS | Metrics & More | Article Recommendations | Supporting Information

ABSTRACT: Quick and accurate molecular diagnostics in protein detection can greatly benefit medicine in disease diagnosis and lead to positive patient outcomes. However, specialized equipment used in clinical laboratories often comes with trade-offs between operation and function serving a single role for very specific needs. For example, to achieve high analytical sensitivity and specificity, instruments such as high-performance liquid chromatography and/or liquid chromatography−mass spectrometry use a complex instrument design and require thorough training of the users. On the other hand, simple tests such as protein detection in urinary tract infection using dip-stick assays provide very quick results but suffer from poor analytical sensitivity. Here, we present an application study for the 3D particle counter technology, which is based on optical confocal detection in order to scan large sample volumes (0.5−3 mL) in glass cuvettes, that aims to close the gap between analytical sensitivity and turnover assay time and simplify protein detection by adopting bead-based immunoassays. Combining the 3D particle counter technology with bead-based immunoassays, a subpicomolar limit of detection—ranging from 119 to 346 fM—was achieved within 3.5-hour assay time for recombinant mouse interleukin 6 detection. As an alternative instrument to a flow cytometer, the 3D particle counter takes advantages of bead-based immunoassays and provides unique accessibility and flexibility for users.

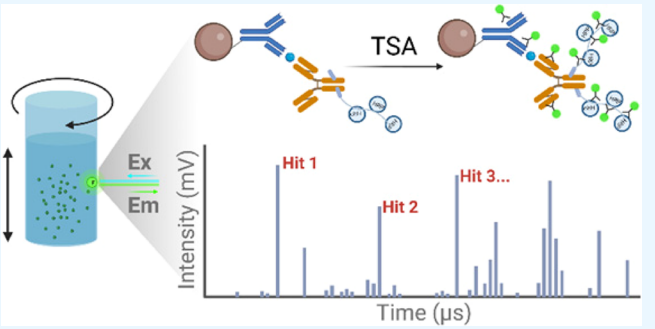

INTRODUCTION

Many traditional diagnostic tests, though instrumental in providing some information during the course of discovery of disease and treatment, employ methods with limited sensitivity and specificity, which only allow physicians to diagnose and empirically treat disease which has already progressed, sometimes up to or beyond points of irreparable physiological damage. Sensitive and specific detection of proteins and other biomolecules, especially at the single-molecule level, would tremendously improve disease prognosis by catching diseases at earlier time points. Such improvements would allow more specific and therefore more efficacious treatment for diseases. Fluorescence immunoassays (FIAs) detect the presence of analytes via a signal change resulting from the direct binding of the analyte to the detection element or in a sandwich format, where a second affinity reagent carries a signal-generating label. While signal amplification schemes such as immunopolymerase chain reaction[1] and immunorolling circle amplification[2] can be used to boost assay sensitivity, the nonzero background of fluorescence curbs the lower limit of detection (LOD).

Digital FIAs can effectively lower the LOD by sample partitioning of protein molecules individually into water-in-oil droplets (droplet volumes can range from ∼0.5 fL to ∼2 pL)[3] or femtoliter-sized wells[4] to spatially confine the amplified signal resulting from single molecules. Positive fluorescent droplets or wells can thus be reliably distinguished using the instrument and reagent-induced background noise renders the measurement vastly independent of background variations. Furthermore, due to the reduced reaction volumes, these methods can save both sample and reagent volume and minimize waste. However, these water-in-oil microfluidic droplets and femtoliter arrays require specialized devices for droplet generation or microwell fabrication, resulting in large and complicated measurement systems.

Alternatively, protein detection at a single analyte level can be achieved by concentrating the amplification reaction products on the surfaces of microbeads. Recently, Akama et al.[5] used a tyramide signal amplification (TSA) system in which single protein molecules were captured on freely moving beads and labeled with horseradish peroxidase (HRP) via a sandwich immunoassay format. Biotinylated tyramides can react with HRP converting them into tyramide radicals,[6] which then accumulated onto beads with labeled HRPs. Subsequently, streptavidin (SA)-dye conjugates were used to bind and fluorescently light up biotin molecules deposited on beads to indicate such beads successfully captured the analyte. While this approach greatly reduces assay complexity by not requiring

Received: July 24, 2022
Accepted: September 21, 2022
Published: October 13, 2022

droplets or microstructured plates, a flow cytometer was needed for absolute counts of positive beads.

Here, we present a simple yet robust bead-based immunoassay for protein detection in large sample volumes of 0.5−3 mL using our 3D particle counting system.[7−9] By eliminating the need for fluid flow and employing relatively simple optical instrumentation, the 3D particle counter positions itself as a cost effective and less complex alternative for target detection compared to a flow cytometer. The 3D particle counter has been designed to quantify fluorescently labeled particles in liquid matrices. At the fundamental basis, this instrument is an inverted fluorescence confocal microscope similar to a flow cytometer. However, unlike the flow cytometer, which uses the scattering of light as well as the emission of fluorescence to detect particles moving in a directed fluid stream, the 3D particle counter analyses samples within a self-contained vial using the principles of fluorescence confocal microscopy. In collaborative studies, the previous applications of the 3D particle counter demonstrating the detection of rare targets in large sample volumes include bloodstream infections and liquid biopsy.[10,11]

As a proof-of-concept, we focused on the detection of interleukins, a large group of cytokines important for cell−cell communications, regulation of the immune responses, hematopoiesis, homeostasis, acute-phase reactions, and many other aspects in biology in general. Specifically, we aimed at detecting interleukin 6 (IL-6) and interleukin 7 (IL-7) as target analytes for the assay development. IL-6, also known as B-cell stimulatory factor-2[12] and interferon beta-2,[13,14] is an interleukin that can act as both anti-inflammatory myokine and proinflammatory cytokine. IL-6 has been found to play a role in the pathology of many diseases such as osteoporosis,[15] rheumatoid arthritis,[16] multiple myeloma,[17] AIDS,[18] mesangial proliferative glomerulonephritis,[19] psoriasis,[20] sepsis,[21] and, most recently, COVID-19.[22] In the case of IL-7, it plays a role in the development of not only B cells and T cells but also innate immune cells such as natural killer cells (for a review, see[23]). IL-7 is also associated with autoimmune diseases such as multiple sclerosis[24] and rheumatoid arthritis.[25]

For these interleukin targets, specific capture antibodies were first conjugated on carboxylic acid functionalized magnetic beads through 1-ethyl-3-[3-dimethylaminopropyl]-carbodiimide hydrochloride (EDC) activation. Specifically, the assay solution contained the target analyte, magnetic beads conjugated with capture antibodies, and biotinylated detection antibodies, to perform a sandwich immunoassay on the magnetic beads. After the SA-poly-HRP incubation, downstream TSA of fluorescence labels was performed, which allowed us to achieve a subpicomolar LOD by 3D particle counting. The current assay can be completed within 3.5 h, which is mainly composed of 1 h for the bead-based immunoassay and 2 h for the TSA reagent incubation period. The sample preparation (reagent incubation time) can be modified, with potential for further reduction in the assay time. The combination of droplet-free digital protein detection with 3D particle counting could serve as a point-of-care (POC) test in environments where flow cytometers are too expensive and too complex to operate and maintain for routine clinical testing.

MATERIALS AND METHODS

Conjugation of Capture Antibodies to Magnetic Beads. To conjugate capture antibodies to magnetic beads, Dynabead M270 Carboxylic Acid magnetic beads (Thermo Fisher Scientific, Waltham, MA) were used. The antibody conjugation protocol used in this study was based on both the literature[26,27] and the manufacture's protocol. For mouse IL-6 and human IL-7 detection, two capture antibodies, Ultra-LEAF Purified antimouse IL-6 MP5-20F3 (BioLegend, San Diego, CA) and Ultra-LEAF Purified antihuman IL-7 BVD10-40F6 (BioLegend, San Diego, CA), were purchased and conjugated to the magnetic beads. First, 100 μL aliquots of magnetic beads were pulse vortexed and shaken for at least 30 min at room temperature on a rocker to remove bead aggregates. The beads were then washed with 500 μL of 50 mM MES pH 6 three times using a 12-Tube Magnetic Separation Rack (New England Biolabs, Ipswich, MA). To activate the carboxylic acid functional groups on the beads, 1 mg of EDC (Thermo Fisher Scientific, Waltham MA) was dissolved in 100 μL of 50 mM MES pH 6 and added to the magnetic beads after the final wash. The beads were activated by incubating with EDC for at least 30 min at room temperature on a shaker. Then, the capture antibody's storage buffer was also exchanged with 50 mM MES pH 6 before conjugation. To exchange the storage buffer, Vivaspin 50 K MWCO (Sartorius Stedim Biotech, Göttingen, Germany) columns were used. Maintaining 500 μL working volume, the buffer was exchanged three times by centrifuging the column at 14,000 × g for 5 min each. After the buffer exchange, the antibody concentration was measured using a NanoDrop 2000 spectrophotometer (Thermo Fisher Scientific, Waltham, MA) by measuring A280, which was used to calculate the protein concentration in mg/mL. At least 40 μg of the capture antibody was used for antibody conjugation. The working volume of the antibody conjugation was adjusted to 200 μL using 50 mM MES pH 6 and directly added to the activated magnetic beads. The buffer exchanged capture antibodies and the activated magnetic beads were incubated in a 1.5 mL tube for 2 h on a shaker. After incubation, the supernatant was removed, and 100 μL of 10× TBST (G BioSciences, St. Louis, MO) was added to the magnetic beads and incubated on a shaker for 15 min at room temperature to quench the reaction. The beads were washed three times with 500 μL of 1× PBST (G BioSciences, St. Louis, MO) and reconstituted with 100 μL of 1× PBST (G BioSciences, St. Louis, MO). The final concentration of the antibody conjugated magnetic beads was considered identical to the bead concentration provided by the manufacturer, that is 2 × 10^9 beads/mL.

Bead-Based Immunoassay for Analyte Titration Experiments. The bead-based assay protocol was based on previous literature.[27] In this study, recombinant mouse IL-6 and human IL-7 (BioLegend, San Diego, CA) were used as the analytes. The approximate molecular weights of the recombinant mouse IL-6 and human IL-7 were 25.0 and 18.9 kDa, respectively. Using the Qubit Protein Assay Kit (Thermo Fisher Scientific, Waltham, MA), the concentration of the recombinant proteins was measured in mg/mL, which was then converted into molar concentration. The stock molar concentrations of the recombinant mouse IL-6 and human IL-7 were calculated to be 13.1 and 14.7 μM, respectively. To perform titration experiments, each analyte was serially diluted using Superior Blocking Buffer (G Biosciences, St. Louis, MO) and added to a 96-well microplate (Qiagen, Hilden, Germany) with a working volume of 100 μL for each concentration point. Typically, the maximum analyte concentration was set to be 200 pM, and 6−10 concentration points were tested in either

https://doi.org/10.1021/acsomega.2c04666
ACS Omega 2022, 7, 37714−37723

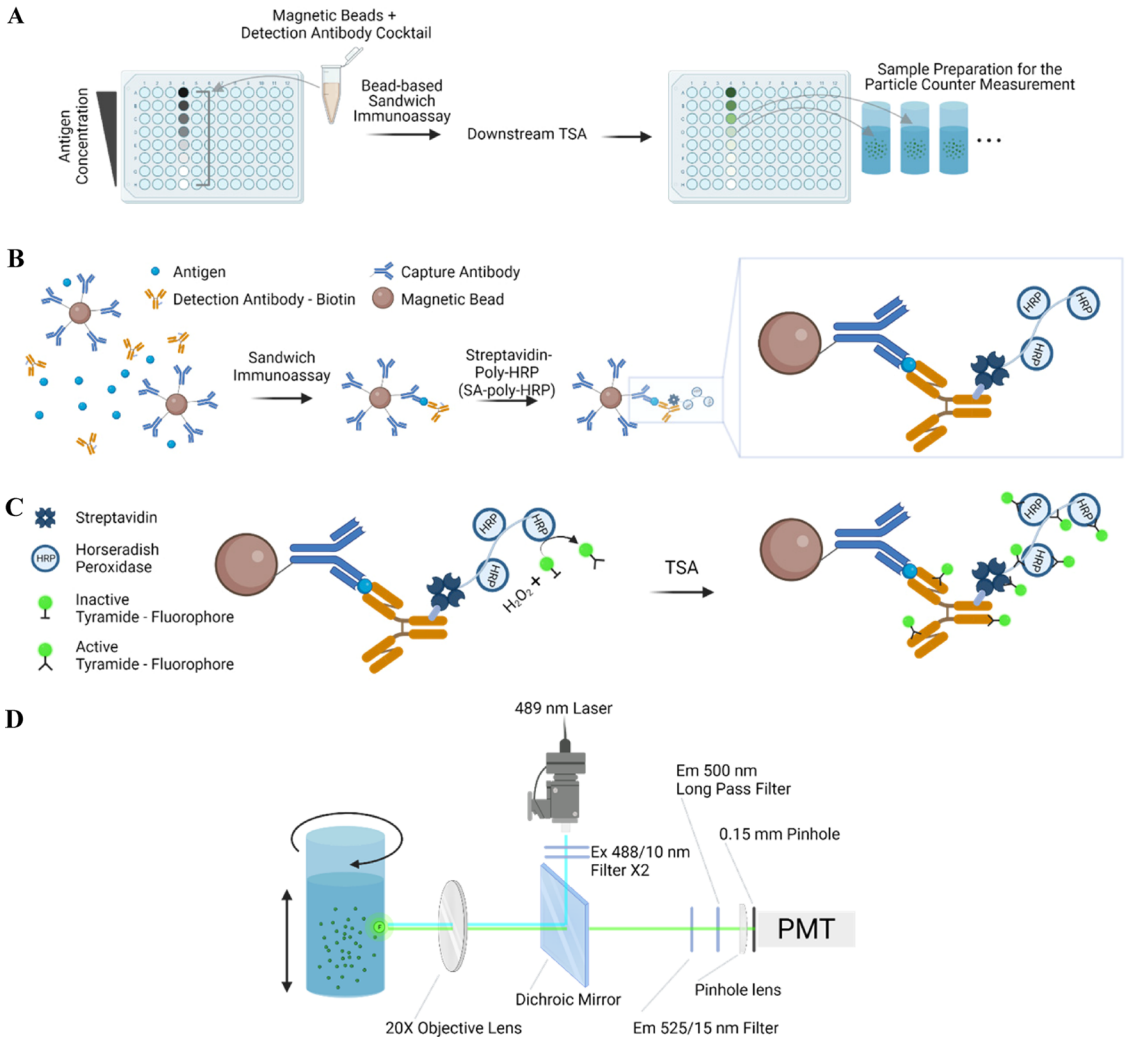

Figure 1. Graphic summary of sample preparation, bead-based sandwich immunoassay, and 3D particle counter optical setup. Target antigens were serially diluted on a 96-well plate. Then, a cocktail of magnetic beads conjugated with specific capture antibodies and detection antibodies was dispensed into each well to perform the sandwich immunoassay. Finally, TSA was performed using SA-poly-HRP to directly deposit fluorophore molecules on the protein complex to develop a fluorescence signal. (A) A general workflow of sample preparation for the particle counter is shown. (B) The bead-based sandwich immunoassay scheme is shown. Capture antibodies were conjugated to magnetic beads. For each bead, the sandwich immunoassay takes a place on the bead surface. SA-Poly-HRP molecules then bind to biotinylated detection antibodies, providing the enzymatic reaction for the immunoassay. (C) TSA on the magnetic bead after sandwich immunoassay is shown. HRP molecules convert tyramide−fluorophore conjugates into radicals, where these highly reactive radicals bind to tyrosine residues on the protein complex and deposit a large number of fluorophores on the bead. (D) The optical configuration of the 3D particle counter technology is similar to a standard confocal microscope setup. A schematic description of the single channel optical setup installed in the 3D particle counter is shown here. Clean-up filters for both excitation and emission wavelengths were applied to improve the SNR in measurements during the raw data acquisition. A relatively small pinhole size (0.15 mm) was used to optimize magnetic bead detection. This figure was created with BioRender.com

2-fold or 5-fold serial dilutions. At least two negative controls without analytes were tested with 100 μL of the same blocking buffer for each experiment. Once the diluted analytes were added to the 96-wells plate, a cocktail of the magnetic beads that were conjugated with specific capture antibodies and detection antibody was prepared. For the detection antibodies, biotinylated antimouse IL-6 MP5-32C11 (BioLegend, San Diego, CA) and biotinylated antihuman IL-7 BVD10-11C10 (BioLegend, San Diego, CA) were used. For each analyte concentration point, a cocktail composed of the diluted detection antibody and the magnetic beads was added. Specifically, 10 μL of 100-fold diluted detection antibody and 10 μL of 5×10^5 preconjugated magnetic beads were added to each well to perform the immunoassay. The plate was shaken for 1 h at room temperature. Then, the beads were washed three times with 100 μL of 1× PBST (G Biosciences, St. Louis, MO). To develop the fluorescence signal on the magnetic beads after forming immunocomplexes, either Alexa Fluor 488-conjugated Streptavidin (SA-AF488) (Jackson ImmunoResearch, West Grove, PA) or Pierce Streptavidin Poly-HRP (SA-poly-HRP) (Thermo Fisher Scientific, Waltham, MA) was added to the magnetic beads for 10 min on a shaker at room temperature. These SA conjugates were diluted with a dilution factor of 10^4 in a working volume of 100 μL. In the case of the SA-poly-HRP treated beads, a downstream TSA step was performed to develop the fluorescence signal, as depicted in Figure 1. After fluorescence signal development, the magnetic beads were added to glass cuvettes filled with 2 mL of 1× PBST (G Biosciences, St. Louis, MO) for 3D particle counting. Before fluorescence detection with the

https://doi.org/10.1021/acsomega.2c04666
ACS Omega 2022, 7, 37714−37723

particle counter, these glass cuvettes containing the bead samples were sonicated for 15−30 s to remove bead aggregates.

Bead-Based Immunoassay to Confirm the Capture Antibody Conjugation. To compare the effect of different amounts of capture antibody used for conjugation on the number of hits and fluorescence intensities measured with the 3D particle counter, the same bead-based immunoassay protocol described above with some modifications was followed. 100 μL Superior Blocking Buffer (G Biosciences, St. Louis, MO), 1 μL stock recombinant mouse IL-6, 1 μL stock detection antibody, and 5 × 10^5 magnetic beads preconjugated with two different amounts of the antimouse IL-6 capture antibodies, 47.6 and 52.2 μg, were separately added in 1.5 mL tubes and incubated on a shaker for 30 min at room temperature. Negative controls did not contain 1 μL of the stock analyte. Then, the beads were washed three times with 1× PBST (G Biosciences, St. Louis, MO) and treated with diluted SA-AF488 with a dilution factor of 10^3 in a working volume of 100 μL for 10 min on a shaker at room temperature. The beads were again washed three times and added into glass cuvettes containing 2 mL of 1× PBST (G Biosciences, St. Louis, MO) for measurement with the 3D particle counter.

Downstream TSA. To perform TSA on the magnetic beads, Alexa Fluor 488 Tyramide SuperBoost Kit, SA (Thermo Fisher Scientific, Waltham, MA) was used, following the manufacturer's protocol with some modifications. Instead of using 100× reagents per manufacturer's protocol, tyramide reagent and H_2O_2 were further diluted to 10× using DMSO and UltraPure DNase/RNase-Free Distilled Water (Thermo Fisher Scientific, Waltham, MA), respectively. To prepare 1× reaction buffer, 1× TBST (G Biosciences, St. Louis, MO) was used. To prepare 1× reaction stop reagent, 1× PBST (G Biosciences, St. Louis, MO) was used. Tyramide reagent was incubated with the magnetic beads with a complete immunocomplex containing SA-poly-HRP at room temperature for 2 h without shaking.

Particle Counting and Data Normalization. Positive beads were counted with a modified Quanta particle counter (ISS, Champaign, IL) as previously described.[9] A schematic of the particle counter is shown in Figure 1D. Briefly, the sample was illuminated with the beam of a diode laser (489 nm, ISS) that was spectrally cleaned with two band pass filters (488/10 nm, Semrock, Rochester, NY), reflected off a dichroic mirror (zt488rdc, Chroma, Bellows Falls, VT), and focused into the sample cuvette with a 20×, NA 0.4 objective lens (Newport, Franklin, MA). From the resulting excitation volume, fluorescence was picked up by the same lens, separated from scattered excitation light with a band pass filter (525/15 nm, Semrock), and spatially filtered with a 0.15 mm diameter pinhole (Thorlabs, Newton, NJ) before detection with a photomultiplier (65816, Hamamatsu) at a sample rate of 64 kHz. Before the measurement, the excitation/detection arm was horizontally translated to optimize the position of the observation volume in the sample cuvette. During data collection (1 min per specimen), the sample was rotated at 200 rpm and axially translated at 2 mm/s to explore a large portion of the fluid volume of 2 mL. A correlation filter was used to detect positive signals ("hits") in the fluorescence time trace using SimFCS software (freely available at: https://www.lfd.uci.edu/globals/). The average number of hits from no antigen controls was used to normalize the hits from positive beads, reporting signal-to-noise ratio (SNR) in the analyte titration experiments.

LOD and Limit of Quantification Calculation. The normalized data (S/N) obtained from the analyte titration experiments were fitted with a 5-parameter logistic regression model (5PL-regression) using Origin Pro software (OriginLab, Northampton, MA). The LOD was calculated by finding the X value from 2× A_{min} Y value. The limit of quantification (LOQ) was calculated by finding the X value from 10× A_{min} Y value.

Confocal Imaging. The magnetic beads were retrieved from the glass cuvettes filled with 2 mL 1× PBST (G Biosciences, St. Louis, MO) using a magnetic rack, where the working volume was reduced to 50 μL. Then, 5 μL of the beads were sandwiched between two glass cover slips of ∼0.17 mm thickness each and imaged with a LSM710 laser scanning microscope (Zeiss, Jena, Germany) equipped with a 40×, NA 1.2 water immersion objective. Fluorescence was excited with 488-nm light and detected with a photomultiplier detector in a band of 510−550 nm through a pinhole set to one Airy unit. Simultaneously, in a second channel, transmission light was detected. Images of 512 × 512 pixels were scanned with a sample pixel size of 140 or 420 nm and a pixel dwell time of 6.3 μs. The fluorescence signal along a horizontal line on the positive beads was manually measured using ImageJ (National Institutes of Health, Bethesda, MD) built-in function.

Fluorescence Intensity Standard Bead Test for the 3D Particle Counter Optimization. To characterize the particle counter performance prior to testing the magnetic bead-based immunoassay, fluorescence intensity standard beads, the Dragon Green Intensity Standard kit (Bangs Laboratories, Inc., Fishers, IN), were measured with the 3D particle counter. In the following, we abbreviated the Dragon Green beads as DG with the corresponding fluorescence intensity levels from 1 to 5 (i.e., DG1 being the dimmest to DG5 being the brightest). This kit contained a total of five different fluorescence intensities, where the relative fluorescence intensities were provided as percentages. About 5 × 10^4 DG beads were tested on the particle counter to all fluorescence intensity levels. To examine the robustness and to optimize the particle counter for bead detection (bead size from 3 to 8 μm), 5 × 10^4 DG2 beads were added to three different solutions in glass cuvettes: 2 mL 1× PBST, 2 mL 0.5 nM Pierce Biotin−Fluorescein Conjugate (Thermo Fisher Scientific, Waltham, MA), and 5.0 nM Pierce Biotin−Fluorescein Conjugate (Thermo Fisher Scientific, Waltham, MA). These samples were then tested against pinholes with four different diameters: 0.1, 0.15, 0.33, and 0.5 mm.

RESULTS

Bead-Based Immunoassay and the 3D Particle Counter. In the capture bead assay, microparticles were used to spatially focus the biochemical reactions needed to detect the presence of the target analyte with high efficiency. This was achieved with the general sample preparation for the 3D particle counter as illustrated in Figure 1. Specifically, our approach was implemented as a sandwich type assay (Figure 1B,C). For each interleukin target, a serial dilution of the analyte was performed, where each analyte concentration was tested with an identical bead-based sandwich immunoassay. After performing the sandwich immunoassay on the beads, tyramide−fluorophore (Alexa Fluor 488) was added to react with multiple HRPs on positive beads. The positive beads that successfully captured the target analyte turned the tyramide−

https://doi.org/10.1021/acsomega.2c04666
ACS Omega 2022, 7, 37714−37723

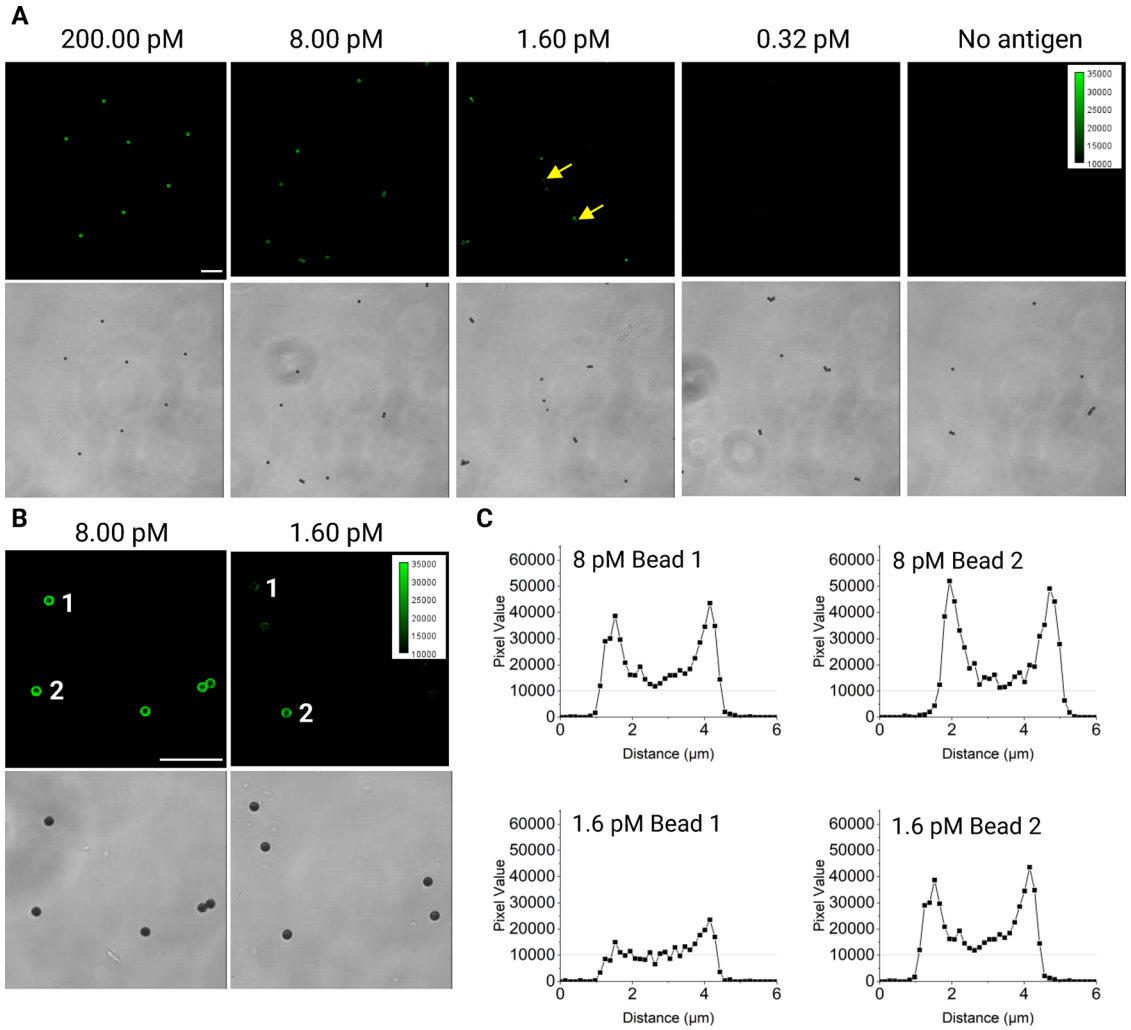

Figure 2. Confocal images of mouse IL-6 captured magnetic beads and fluorescence signal quantification. To validate protein capture using the antibody conjugated magnetic beads, confocal microscopy was used to validate the fluorescence signals. (A) 20× images of magnetic beads after treating with diluted recombinant mouse IL-6 are shown. Both fluorescence and brightfield images were obtained. Some beads lost fluorescence signals (yellow arrows) below 1.6 pM mouse IL-6 concentration. Scale bar, 20 μm. (B) To observe the fluorescence signals on the beads more closely, 40× fluorescence and brightfield images of magnetic beads were obtained. Shown are example beads after treating with 8 and 1.6 pM of mouse IL-6. Scale bar, 20 μm. (C) Relative fluorescence signals (pixel values) were measured across the beads (bead 1 and bead 2) from the 40× fluorescence images. Both bead 1 and bead 2 from the 8 pM mouse IL-6 concentration showed a halo-like ring fluorescence pattern, indicating protein capture on the entire surface of the magnetic beads. In the case of 1.6 pM, only bead 2 showed a halo-like ring fluorescence pattern, whereas bead 1 showed a fluorescence signal on the right side of the bead only, which may indicate a partial protein capture on the surface. For visualization, the color scale of the fluorescence images was set from 10,000 to 35,000 cts.

fluorophore into tyramide radicals, which then immediately deposit near the SA-poly-HRP label. The exponential tyramide-based signal amplification is key to generating a strong fluorescence signal. In principle, a single target molecule tying a HRP complex to a capture bead could be sufficient to generate a positive, detectable signal. The number of positive beads can then be digitally counted to quantify the analyte concentration present in the sample by the 3D particle, where its specific optical setup used in this study is illustrated in Figure 1D.

Benchmarking against a Confocal Microscope. To investigate and verify the fluorescence signal after mouse IL-6 capturing and amplification, a small amount of the sample was deposited onto microscope slides and subjected to high resolution confocal imaging. Example fluorescence and bright-field images are shown in Figure 2A, representing four IL-6 concentration points: 200, 8, 1.6, and 0.32 pM. Below 8 pM, a range of fluorescence intensities were observed within the positive bead population. Most of the positive beads showed a halo-like ring of fluorescence, indicating the tyramide−fluorophore conjugates were successfully deposited on the entire surface of the magnetic bead after capturing the target analyte. However, at 1.6 pM, some beads (e.g., bead 1 in Figure 2B) showed only a partial fluorescence signal on the surface, compared to the other beads (e.g., bead 2 in Figure 2B) which generated a halo-like ring fluorescence signal, whereas, at 8 pM, all beads clearly showed a halo-like fluorescence signal. The fluorescence intensities along the cross sections of these beads were quantified as shown in Figure 2C. While imaging provides a means of detecting positive beads, only a few microliters of solution can be probed at a time, significantly limiting throughput. Also, if the number of positive beads is low, there may not be a single particle within the field of view, limiting the lower LOD in larger

https://doi.org/10.1021/acsomega.2c04666
ACS Omega 2022, 7, 37714−37723

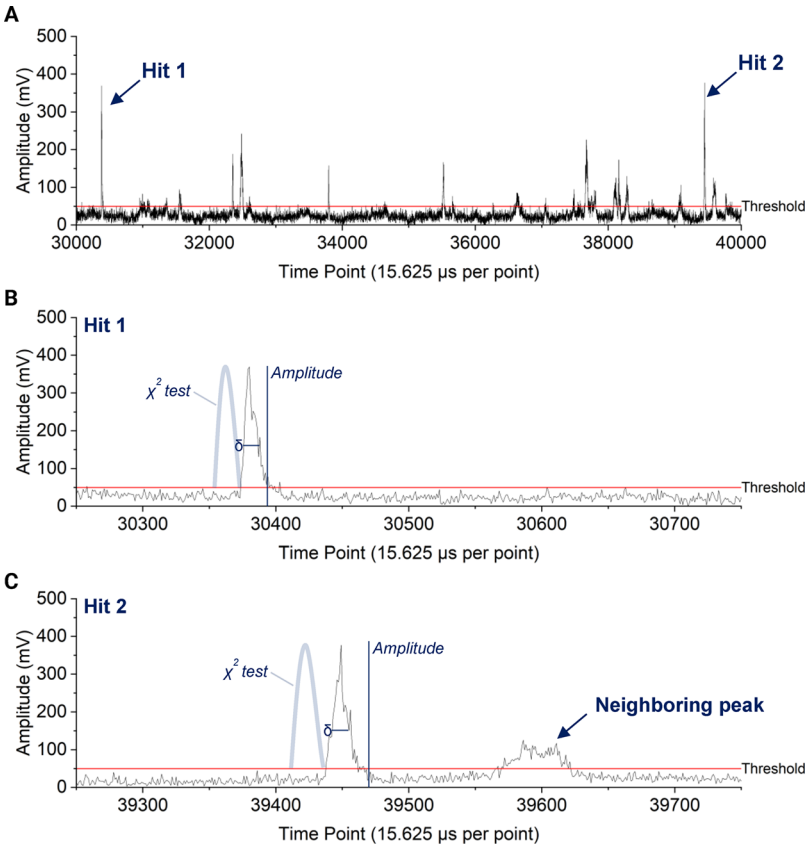

Figure 3. Process to determine positive peaks from raw data. Raw data acquired from the particle counter were processed by applying the curve fitting algorithm provided from the SimFCS software (Laboratory for Fluorescence Dynamics, CA). There are three main parameters that determine "positive" peaks as hits. First, SDV (δ) determines the peak width parameter. Second, the amplitude threshold determines the PMT signal cutoff value in mV, which therefore determines the fluorescence signal from the magnetic bead that has successfully captured the target analyte. Third, the p-value set for the χ^2 test determines the fitness of the measured curve to a theoretical Gaussian curve; here, the theoretical Gaussian curves are simply shown as illustration for comparison to the raw data. All three conditions must be satisfied to be determined as a positive peak (a hit). (A) Representative raw data acquired from detecting mouse IL-6 at 200 pM are shown. Here, the raw data acquired from 30,000 to 40,000 time point are shown. The red line represents the amplitude threshold (50 mV). Within this time period, two positive peaks (two hits) were detected: Hit 1 and Hit 2. The other peaks shown between Hit 1 and Hit 2 were discarded from the calculation. Therefore, this particular measurement yielded about two hits per 15.6 μs. Usually, each specimen (cuvette sample) was measured for a total of 30−60 s. (B) A close-up of Hit 1 is shown. (C) A close-up of Hit 2 and the neighboring peak is shown. The neighboring peak does not satisfy the SDV threshold and χ^2 test although its peak amplitude is above the 50 mV threshold; accordingly, this neighboring peak is not considered as a hit.

sample volumes. Additionally, reduction of the liquid volume, for example, by centrifugation and/or size exclusion chromatography, often leads to sample loss and can disturb and strip-off captured proteins from the bead surface.

To validate that the 3D particle counter can properly detect and count fluorescence microparticles, side-by-side operation of the 3D particle counter and the confocal microscope was performed, resulting in a comparable performance in detecting the fluorescence intensities of standard beads (Figure S1). To minimize the variability in the comparison, 8 μm polystyrene-based beads filled with Dragon Green dye (DG beads), whose maximum excitation and emission wavelengths were 480 and 520 nm, respectively, were used because these beads were compatible with the optical setup of the 3D particle counter tested in this study (Figure 1D). These DG beads were grouped by five different fluorescence intensity levels (DG 1−5). DG1 was the dimmest, and DG5 was the brightest. The confocal fluorescence images of the DG beads, with their relative fluorescence intensity percentages obtained from the manufacturer, are shown in Figure S1A. The DG2 seemed to be the limit for visualization with the confocal microscope.

Then, the same set of the DG beads was tested on the 3D particle counter, where the bead fluorescence intensities were measured in mV (Figure S1B), and the number of hits (Figure S1C) was counted that was identical to the number of data points in the fluorescence intensity analysis. For each DG bead, five independent measurements were performed to calculate the coefficient of variation in percentage (CV %) (Figure S1D). The DG2 resulted in the highest CV % of 25.9%, whereas the brighter DG beads resulted in a much lower CV % than expected. The dimmest DG1 resulted in a lower CV % than the DG2 did. An explanation of the low CV % of the DG1 may be the noisy signal (i.e., the DG1 measurements mostly included background rather than true signals). In accordance with the confocal microscope images, the DG2 seems to be the limit using the 3D particle counter, although some DG1 beads showed very weak fluorescence intensities. In summary, we found that the 3D particle counter was able to provide data comparable to the confocal microscope, but at a much higher throughput. The signals detected from the DG1 beads on the 3D particle counter may have included potential aggregates,

https://doi.org/10.1021/acsomega.2c04666
ACS Omega 2022, 7, 37714−37723

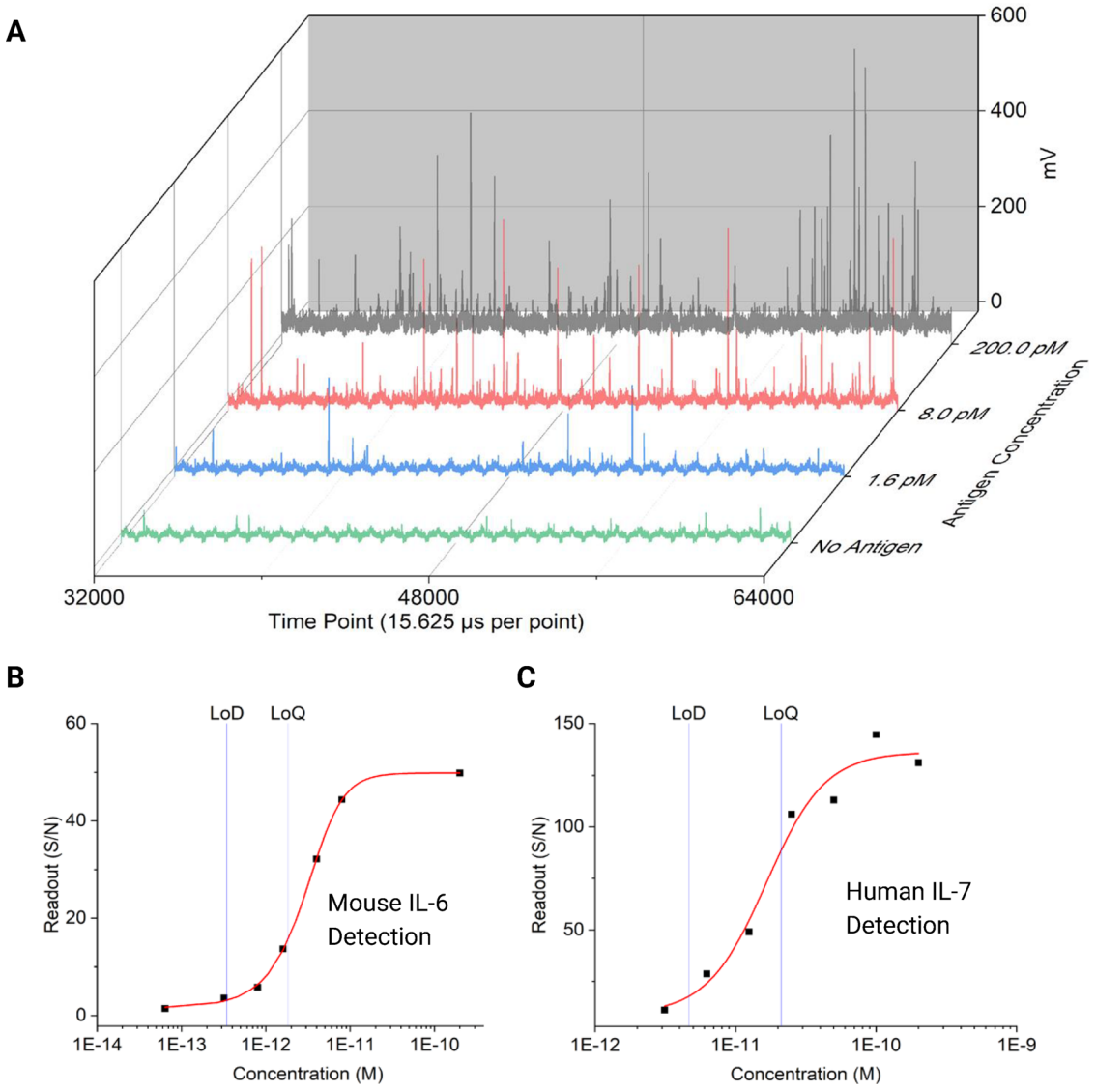

Figure 4. Protein detection on the 3D particle counter. Using magnetic beads conjugated with specific capture antibodies against mouse IL-6 and human IL-7, a bead-based immunoassay was performed. The fluorescence signal was directly obtained from the magnetic beads by downstream TSA. The beads were scanned by the 3D particle counter at different analyte concentrations. For each titration experiment, a single measurement for each concentration point per target was performed. At least two independent titration experiments were performed. (A) Representative raw data of the fluorescence signal intensity of each magnetic bead passing through the confocal volume of the 3D particle counter at a given period of measurement time are shown. Specifically, half a second of data after capturing mouse IL-6 at three different concentrations (1.6, 8.0, and 200.0 pM) and the negative control are shown. After processing the raw data using the correlation filter algorithm using the SimFCS software (Laboratory for Fluorescence Dynamics, CA), the number of positive peaks ("hits") was counted. (B) A representative mouse IL-6 titration curve after fitting with a 5PL logistic regression model is shown. Two independent experiments resulted in a LOD of 119 and 346 fM. (C) A representative human IL-7 titration curve after fitting with a 5PL logistic regression is shown. Two independent experiments resulted the LODs of 4.65 and 5.51 pM. For both titration curves, the normalized positive peak number from each analyte concentration (S/N) was used as the readout.

which required further investigation and optimization of the instrument.

Optimization of the 3D Particle Counter. Next, to optimize the 3D particle counter, specifically, to improve SNR of the instrument, we aimed to test four different pinhole sizes, 0.1, 0.15, 0.33, and 0.5 mm. In order to mimic cytokine detection in clinically relevant (e.g., blood) samples containing autofluorescent components such as cellular debris,[28] which may interfere with positive signal detection, biotin−polyethylene glycol (PEG)−fluorescein isothiocyanate (FITC) molecules were added as a simulated fluorescent background to the glass cuvettes. Since both fluorescein and DG dye share similar excitation/emission spectra (maximum excitation and emission wavelengths are 490 and 525 nm for fluorescein, and 480 and 520 nm for Dragon Green), peak detection demonstrated the specificity of the 3D particle counter for targets. Then, we tested these conditions in all possible combinations to detect the DG2 beads on the 3D particle counter, which were previously found to be the limit on both the confocal microscope and the 3D particle counter (Figure S2). After testing four different pinhole sizes, we found that the 0.1 mm pinhole showed no peak detection even from the positive control. This is because the 0.1 mm pinhole may have been too small to collect enough photons from the DG2 emission to be recorded by the photomultiplier tube (PMT) detector. Instead, the 0.15 mm pinhole was optimal because it

https://doi.org/10.1021/acsomega.2c04666
ACS Omega 2022, 7, 37714−37723

Table 1. Summary Statistics of Protein Detection with the 3D Particle Counter[a]

experiment	target	number of concentration points	minimum analyte concentration (M)	maximum analyte concentration (M)
1	Mouse IL-6	6	6.40×10^{-14}	2.00×10^{-10}
2	Mouse IL-6	7	6.40×10^{-14}	2.00×10^{-10}
3	Human IL-7	7	3.13×10^{-12}	2.00×10^{-10}
4	Human IL-7	10	3.91×10^{-13}	2.00×10^{-10}

experiment	Amin (S/N)	LOD (M)	LOQ (M)	R-Square
1	1.192	$1\ 19 \times 10^{-13}$	4.17×10^{-13}	0.998
2	1.564	3.46×10^{-13}	1.84×10^{-12}	0.999
3	8.862	4.65×10^{-12}	2.11×10^{-11}	0.976
4	3.352	5.51×10^{-12}	1.07×10^{-11}	0.981

[a]LOD and LOQ were calculated using A_{min} ×2 and ×10, respectively.

enabled reliable peak detection from the DG2 beads even in the presence of a relatively high green fluorescent background of 5.0 nM biotin−PEG−FITC. Accordingly, we used the 0.15 mm pinhole for subsequent experiments.

Investigation for Positive Peak Detection. After optimizing the 3D particle counter with the DG fluorescence standard beads, we further investigated the positive peak (hit) detection of the magnetic bead-based immunoassay capturing recombinant mouse IL-6 (Figure 3). Fluorescence signals from individual beads were analyzed within a confocal volume determined by the optical configuration of the 3D particle counter. After recording PMT raw data, that is fluorescence intensities from positive beads, SimFCS software was used to analyze the raw data with a correlation filter that defined the shape of positive "hits" with a Gaussian model. The two core parameters used with the (Gaussian) correlation filter were the p-value for the χ^2 test and the peak amplitude threshold in millivolt (mV). In this study, a stringent p-value of 0.02 for the χ^2 test was used to filter out noise and to define the "hits." Generally, a more lenient p-value increased the number of hits from all concentration points, while a more stringent p-value decreased the number of hits (data not shown). Furthermore, we also examined the relationship between the amount of capture antibody used for the bead conjugation and its effect on both peak amplitude and number of hits detected (Figure S3). In the case of the mouse IL-6 capture antibody, two amounts (47.6 and 52.2 μg) were tested for the bead conjugation. Then, these two bead populations were equally treated with the same analyte concentration, and the same immunoassay was performed. Interestingly, a similar number of hits was observed from the two bead populations, but the one treated with 52.2 μg of the capture antibody resulted in a higher fluorescence intensity than the other one treated with 47.6 μg. Accordingly, although we could further titrate the capture antibody amount to pinpoint the minimum amount of the capture antibody needed for the conjugation, we concluded that at least 40.0 μg of the capture antibodies was needed to perform a reliable bead-based immunoassay.

Detection of Recombinant Proteins and Assay Sensitivity. Because the number of beads was constant per sample, the number of detected peaks saturated at high analyte concentrations (digital regime), while the signal amplitudes proportional to the fluorophore and thus analyte density on the bead surface further increased (analog regime). Therefore, a digital regime can be achieved by using a signal amplification method such as TSA. Compared to SA-AF488 treated bead populations without signal amplification, SA-poly-HRP and subsequent TSA treated beads showed a clear trend in amplitude values, following the concentration points (Figure S4). At lower analyte concentrations, there are less fluorophores per bead, thereby reducing the signal amplitude down to the point where more and more beads will no longer produce any (detectable) signal (Figure 4). For the two analytes tested, mouse IL-6 and human IL-7, this lower digital regime offers higher detection sensitivity and is quantified as shown in Figure 4B,C. Two independent titration experiments with a minimum of six concentration points (a single measurement for each concentration point) were tested for both interleukin targets. A negative control, the control without the analyte, was always measured for each experiment, and the resulting number of hits was used to normalize the number of hits from different analyte concentration points, named readout signal-to-noise (S/N). The S/N values from each concentration point for each interleukin target were fitted with a 5PL logistic regression model. For all titration experiments, a good R^2 (>0.95) was observed. The LOD and LOQ were defined as 2× A_{min} (the minimum Y value from the fitted curve) and 10× A_{min}. Detailed summary statistics of the analyte titration experiments can be found in Table 1. In this study, the 3D particle counter approach yielded a LOD in the subpicomolar range for mouse IL-6 and in the single digit picomolar range for human IL-7.

DISCUSSION

Here, we adopted a bead-based immunoassay to the 3D particle counter technology,[7−9] which allowed us to achieve protein detection in the digital regime from bulk solutions. To achieve high fluorescence signals, TSA was applied on the beads after carrying out the immunoassay. In the case of the positive peak detections, although a lenient p-value generally increased the number of hits from all concentration points, this did not improve the analytical sensitivity of the assay (data not shown). The few nonspecific hits recorded from the negative controls were used to normalize the number of hits and to determine the S/N in the analyte titration experiments, where the A_{min} values for the two analytes in this study were all above a S/N of 1. The analytical sensitivity of our assay showed a subpicomolar LOD, where its S/N value was >2.

We note that other technologies in the field of protein detection in the digital regime have achieved subfemtomolar LOD.[4,29] For example, one of the state-of-art digital protein detection technologies are Quanterix single-molecule arrays (SiMoAs), which achieved an extremely sensitive digital ELISA with a LOD of 0.4 fM for prostate-specific antigen detection.[4] Such technology can therefore help physicians in the diagnosis of certain diseases. However, to achieve such extreme analytical sensitivity, complex instrumentation designs including but not limited to femtoliter-sized well fabrication with controlled

https://doi.org/10.1021/acsomega.2c04666
ACS Omega 2022, 7, 37714−37723

surface chemistry and optimization of microfluidic systems are required, which will likely increase the cost per sample tested. Another way to achieve high analytical sensitivity in protein detection is to adopt bead-based immunoassay using flow cytometry. To detect fluorescent particles within larger volumes (~0.2 to 2 mL), flow cytometry has been used (for a review, see ref 30). Yet, the fluidic system of such instruments involving pumps, tubing, and interconnectors adds complexity and, thus, requires regular and careful cleaning and maintenance by trained personnel.

As a simple and robust alternative to a flow cytometer, we have previously developed the 3D particle counter.[7−9] While flow cytometry spatially separates individual particles by flowing them through a thin tube, our 3D particle counting system uses focused illumination in combination with confocal detection to optically confine the observation volume which enables the detection of individual particles in a bulk solution (Figure 1D). The system consists of a laser source that is focused into a spot of a few tens of micrometers in diameter with an objective lens. Fluorescence from this spot is then passed through a pinhole to reject out-of-focus light before detection with a highly sensitive photomultiplier detector. This is achievable because the rotation of a cuvette containing the bead samples allows the beads to constantly spread outward. To note, fluorescence of a glass cuvette is indeed detected during raw data acquisition; however, such background fluorescence is considered and rejected as the correlation filter detects positive peaks (note the recorded data under the amplitude threshold shown in Figure 3). Therefore, the advantages of the 3D particle counter are rather found in the simplicity of the instrument and assay design. Key advantages include avoiding complex surface chemistry, droplet generation, and microfluidics to achieve a moderately high LOD.

Accordingly, one main application for the 3D particle counter technology would be to function as a POC device to monitor a patient's analyte level over time; a miniaturized version of the 3D particle counter has already been developed and applied for antibiotic susceptibility tests.[31] Therefore, potential applications include the monitoring of key proinflammation markers such as IL-6 and tumor necrosis factor α in COVID-19 patients with severe symptoms,[32,33] as these cytokines have been previously studied as potential biomarkers to predict the severity and survival of COVID-19 patients.[33] Additionally, the 3D particle counter uses samples confined to a (sealed) container. Therefore, during the measurement, no spillage, clogging, or contamination can occur, and this maintenance-free instrument could be set up in almost any environment.

These advantages of the 3D particle counter also highlight the accessibility of instruments as a critical factor to consider when deploying new diagnostic tests or assays, where developing countries have limited funding and resources to establish and manage centralized laboratories to fight against infectious diseases.[34] For example, to address the accessibility of instruments further, Li et al. developed Octopi, which is an open configurable high-throughput imaging platform for infectious disease diagnosis, specifically to detect malaria parasites, providing a user-friendly system with high sensitivity and specificity.[35] As a result, in the future, we envision the 3D particle counter technology to be adapted to a variety of molecular and cellular assays to fulfill relevant clinical needs with a quick turnover time.

■ ASSOCIATED CONTENT

Supporting Information

The Supporting Information is available free of charge at https://pubs.acs.org/doi/10.1021/acsomega.2c04666.

Benchmarking between a confocal microscope and the 3D particle counter; robustness of the 3D particle counter; antibody amount for bead conjugation and its effect on the bead-based immunoassay; effect of TSA on the bead-based immunoassay (PDF)

■ AUTHOR INFORMATION

Corresponding Authors

Per Niklas Hedde − *Department of Pharmaceutical Sciences, Laboratory for Fluorescence Dynamics, and Beckman Laser Institute & Medical Clinic, University of California, Irvine, Irvine, California 92697, United States;* orcid.org/0000-0002-2994-369X; Email: phedde@uci.edu

Weian Zhao − *Department of Biological Chemistry, Department of Pharmaceutical Sciences, Institute for Immunology, Sue and Bill Gross Stem Cell Research Center, Chao Family Comprehensive Cancer Center, Edwards Life Sciences Center for Advanced Cardiovascular Technology, and Department of Biomedical Engineering, University of California, Irvine, Irvine, California 92697, United States;* orcid.org/0000-0002-7794-9914; Email: weianz@uci.edu

Authors

Sungjun Beck − *Department of Biological Chemistry, University of California, Irvine, Irvine, California 92697, United States*

Donghae Shin − *Department of Biological Chemistry, University of California, Irvine, Irvine, California 92697, United States*

Sun Jin Kim − *Department of Pharmaceutical Sciences, University of California, Irvine, Irvine, California 92697, United States*

Complete contact information is available at: https://pubs.acs.org/10.1021/acsomega.2c04666

Author Contributions

S.B. performed most of the project management, specifically experiment designs, data analysis, and manuscript writing. D.S. participated in performing experiments. S.K. provided guidance on assay chemistry. P.N.H. provided guidance on instrumentation, optics, and data analysis, and participated in manuscript writing. W.Z. conceived the project and supervised the study.

Notes

The authors declare the following competing financial interest(s): W.Z. is a cofounder of Velox Biosystems Inc., Amberstone Biosciences Inc., and Arvetas Biosciences Inc.

■ ACKNOWLEDGMENTS

This work was supported by ZERONE SCIENCES LLC (grant # zs-220126).

■ REFERENCES

(1) Niemeyer, C. M.; Adler, M.; Wacker, R. Detecting antigens by quantitative immuno-PCR. *Nat. Protoc.* **2007**, *2*, 1918−1930.

(2) Schweitzer, B.; Wiltshire, S.; Lambert, J.; O'Malley, S.; Kukanskis, K.; Zhu, Z.; Kingsmore, S. F.; Lizardi, P. M.; Ward, D. C. Immunoassays with rolling circle DNA amplification: a versatile

platform for ultrasensitive antigen detection. *Proc. Natl. Acad. Sci. U. S. A.* **2000**, *97*, 10113−10119.
(3) Shim, J.-U.; Ranasinghe, R. T.; Smith, C. A.; Ibrahim, S. M.; Hollfelder, F.; Huck, W. T.; Klenerman, D.; Abell, C. Ultrarapid generation of femtoliter microfluidic droplets for single-molecule-counting immunoassays. *ACS Nano* **2013**, *7*, 5955−5964.
(4) Rissin, D. M.; Kan, C. W.; Campbell, T. G.; Howes, S. C.; Fournier, D. R.; Song, L.; Piech, T.; Patel, P. P.; Chang, L.; Rivnak, A. J.; Ferrell, E. P.; Randall, J. D.; Provuncher, G. K.; Walt, D. R.; Duffy, D. C. Single-molecule enzyme-linked immunosorbent assay detects serum proteins at subfemtomolar concentrations. *Nat. Biotechnol.* **2010**, *28*, 595−599.
(5) Akama, K.; Shirai, K.; Suzuki, S. Droplet-free digital enzyme-linked immunosorbent assay based on a tyramide signal amplification system. *Anal. Chem.* **2016**, *88*, 7123−7129.
(6) Bobrow, M. N.; Harris, T. D.; Shaughnessy, K. J.; Litt, G. J. Catalyzed reporter deposition, a novel method of signal amplification application to immunoassays. *J. Immunol. Methods* **1989**, *125*, 279−285.
(7) Hedde, P. N.; Abram, T.; Vu, T.; Zhao, W.; Gratton, E. Fluorescence lifetime detection with particle counting devices. *Biomed. Opt. Express* **2019**, *10*, 1223−1233.
(8) Kang, D.-K.; Ali, M. M.; Zhang, K.; Huang, S. S.; Peterson, E.; Digman, M. A.; Gratton, E.; Zhao, W. Rapid detection of single bacteria in unprocessed blood using Integrated Comprehensive Droplet Digital Detection. *Nat. Commun.* **2014**, *5*, 5427.
(9) Altamore, I.; Lanzano, L.; Gratton, E. Dual channel detection of ultra low concentration of bacteria in real time by scanning fluorescence correlation spectroscopy. *Meas. Sci. Technol.* **2013**, *24*, No. 065702.
(10) Abram, T. J.; Cherukury, H.; Ou, C.-Y.; Vu, T.; Toledano, M.; Li, Y.; Grunwald, J. T.; Toosky, M. N.; Tifrea, D. F.; Slepenkin, A.; Chong, J.; Kong, L.; del Pozo, D. V.; la, K. T.; Labanieh, L.; Zimak, J.; Shen, B.; Huang, S. S.; Gratton, E.; Peterson, E. M.; Zhao, W. Rapid bacterial detection and antibiotic susceptibility testing in whole blood using one-step, high throughput blood digital PCR. *Lab Chip* **2020**, *20*, 477−489.
(11) Ou, C.-Y.; Vu, T.; Grunwald, J. T.; Toledano, M.; Zimak, J.; Toosky, M.; Shen, B.; Zell, J. A.; Gratton, E.; Abram, T. J.; Zhao, W. An ultrasensitive test for profiling circulating tumor DNA using integrated comprehensive droplet digital detection. *Lab Chip* **2019**, *19*, 993−1005.
(12) Hirano, T.; Taga, T.; Nakano, N.; Yasukawa, K.; Kashiwamura, S.; Shimizu, K.; Nakajima, K.; Pyun, K. H.; Kishimoto, T. Purification to homogeneity and characterization of human B-cell differentiation factor (BCDF or BSFp-2). *Proc. Natl. Acad. Sci. U. S. A.* **1985**, *82*, 5490−5494.
(13) Weissenbach, J.; Chernajovsky, Y.; Zeevi, M.; Shulman, L.; Soreq, H.; Nir, U.; Wallach, D.; Perricaudet, M.; Tiollais, P.; Revel, M. Two interferon mRNAs in human fibroblasts: in vitro translation and Escherichia coli cloning studies. *Proc. Natl. Acad. Sci. U. S. A.* **1980**, *77*, 7152−7156.
(14) Zilberstein, A.; Ruggieri, R.; Korn, J.; Revel, M. Structure and expression of cDNA and genes for human interferon-beta-2, a distinct species inducible by growth-stimulatory cytokines. *EMBO J.* **1986**, *5*, 2529−2537.
(15) Poli, V.; Balena, R.; Fattori, E.; Markatos, A.; Yamamoto, M.; Tanaka, H.; Ciliberto, G.; Rodan, G. A.; Costantini, F. Interleukin-6 deficient mice are protected from bone loss caused by estrogen depletion. *EMBO J.* **1994**, *13*, 1189−1196.
(16) Nakahara, H.; Song, J.; Sugimoto, M.; Hagihara, K.; Kishimoto, T.; Yoshizaki, K.; Nishimoto, N. Anti−interleukin-6 receptor antibody therapy reduces vascular endothelial growth factor production in rheumatoid arthritis. *Arthritis Rheumatol.* **2003**, *48*, 1521−1529.
(17) Kawano, M.; Hirano, T.; Matsuda, T.; Taga, T.; Horii, Y.; Iwato, K.; Asaoku, H.; Tang, B.; Tanabe, O.; Tanaka, H.; Kuramoto, A.; Kishimoto, T. Autocrine generation and requirement of BSF-2/IL-6 for human multiple myelomas. *Nature* **1988**, *332*, 83−85.
(18) Borges, Á. H.; O'Connor, J. L.; Phillips, A. N.; Rönsholt, F. F.; Pett, S.; Vjecha, M. J.; French, M. A.; Lundgren, J. D.; INSIGHT SMART and ESPRIT Study Groups and the SILCAAT Scientific Committee. Factors associated with plasma IL-6 levels during HIV infection. *J. Infect. Dis.* **2015**, *212*, 585−595.
(19) Horii, Y.; Muraguchi, A.; Iwano, M.; Matsuda, T.; Hirayama, T.; Yamada, H.; Fujii, Y.; Dohi, K.; Ishikawa, H.; Ohmoto, Y. Involvement of IL-6 in mesangial proliferative glomerulonephritis. *J. Immunol.* **1989**, *143*, 3949−3955.
(20) Grossman, R. M.; Krueger, J.; Yourish, D.; Granelli-Piperno, A.; Murphy, D. P.; May, L. T.; Kupper, T. S.; Sehgal, P. B.; Gottlieb, A. B. Interleukin 6 is expressed in high levels in psoriatic skin and stimulates proliferation of cultured human keratinocytes. *Proc. Natl. Acad. Sci. U. S. A.* **1989**, *86*, 6367−6371.
(21) Damas, P.; Ledoux, D.; Nys, M.; Vrindts, Y.; De Groote, D.; Franchimont, P.; Lamy, M. Cytokine serum level during severe sepsis in human IL-6 as a marker of severity. *Ann. Surg.* **1992**, *215*, 356−362.
(22) Gordon, A. C.; Mouncey, P. R.; Al-Beidh, F.; Rowan, K. M.; Nichol, A. D.; Arabi, Y. M.; Annane, D.; Beane, A.; van Bentum-Puijk, W.; Berry, L. R. Interleukin-6 receptor antagonists in critically ill patients with Covid-19. *N. Engl. J. Med.* **2021**, *385*, 1147−1149.
(23) Chen, D.; Tang, T.-X.; Deng, H.; Yang, X.-P.; Tang, Z.-H. Interleukin-7 Biology and Its Effects on Immune Cells: Mediator of Generation, Differentiation, Survival, and Homeostasis. *Front. Immunol.* **2021**, *12*, 5156.
(24) Lundström, W.; Highfill, S.; Walsh, S. T.; Beq, S.; Morse, E.; Kockum, I.; Alfredsson, L.; Olsson, T.; Hillert, J.; Mackall, C. L. Soluble IL7Rα potentiates IL-7 bioactivity and promotes autoimmunity. *Proc. Natl. Acad. Sci. U. S. A.* **2013**, *110*, E1761−E1770.
(25) Van Roon, J. A.; Verweij, M. C.; Wijk, M. W. V.; Jacobs, K. M.; Bijlsma, J. W.; Lafeber, F. P. Increased intraarticular interleukin-7 in rheumatoid arthritis patients stimulates cell contact−dependent activation of CD4+ T cells and macrophages. *Arthritis Rheumatol.* **2005**, *52*, 1700−1710.
(26) Wu, D.; Milutinovic, M. D.; Walt, D. R. Single molecule array (Simoa) assay with optimal antibody pairs for cytokine detection in human serum samples. *Analyst* **2015**, *140*, 6277−6282.
(27) Maley, A. M.; Garden, P. M.; Walt, D. R. Simplified digital enzyme-linked immunosorbent assay using tyramide signal amplification and fibrin hydrogels. *ACS Sens.* **2020**, *5*, 3037−3042.
(28) Aubin, J. Autofluorescence of viable cultured mammalian cells. *J. Histochem. Cytochem.* **1979**, *27*, 36−43.
(29) Gilbert, M.; Livingston, R.; Felberg, J.; Bishop, J. J. Multiplex single molecule counting technology used to generate interleukin 4, interleukin 6, and interleukin 10 reference limits. *Anal. Biochem.* **2016**, *503*, 11−20.
(30) Adan, A.; Alizada, G.; Kiraz, Y.; Baran, Y.; Nalbant, A. Flow cytometry: basic principles and applications. *Crit. Rev. Biotechnol.* **2017**, *37*, 163−176.
(31) Toosky, M. N.; Grunwald, J. T.; Pala, D.; Shen, B.; Zhao, W.; D'Agostini, C.; Coghe, F.; Angioni, G.; Motolese, G.; Abram, T. J. A rapid, point-of-care antibiotic susceptibility test for urinary tract infections. *J. Med. Microbiol.* **2020**, *69*, 52.
(32) Long, Q.-X.; Tang, X.-J.; Shi, Q.-L.; Li, Q.; Deng, H.-J.; Yuan, J.; Hu, J.-L.; Xu, W.; Zhang, Y.; Lv, F.-J.; Su, K.; Zhang, F.; Gong, J.; Wu, B.; Liu, X. M.; Li, J. J.; Qiu, J. F.; Chen, J.; Huang, A. L. Clinical and immunological assessment of asymptomatic SARS-CoV-2 infections. *Nat. Med.* **2020**, *26*, 1200−1204.
(33) Del Valle, D. M.; Kim-Schulze, S.; Huang, H.-H.; Beckmann, N. D.; Nirenberg, S.; Wang, B.; Lavin, Y.; Swartz, T. H.; Madduri, D.; Stock, A. An inflammatory cytokine signature predicts COVID-19 severity and survival. *Nat. Med.* **2020**, *26*, 1636−1643.
(34) McNerney, R. Diagnostics for developing countries. *Diagnostics* **2015**, *5*, 200−209.
(35) Li, H.; Soto-Montoya, H.; Voisin, M.; Valenzuela, L. F.; Prakash, M. Octopi: Open configurable high-throughput imaging platform for infectious disease diagnosis in the field. *BioRxiv* **2019**, DOI: 10.1101/684423.